Generalised Impedance Model of Wireless Links Assisted by Reconfigurable Intelligent Surfaces

Keisuke Konno *Member, IEEE,* Sergio Terranova *Member, IEEE,* Qiang Chen, *Senior Member, IEEE* and Gabriele Gradoni, *Member, IEEE*

Abstract—We devise an end-to-end communication channel model that describes the performance of RIS-assisted MIMO wireless links. The model borrows the impedance (interaction) matrix formalism from the Method of Moments and provides a physics-based communication model. In configurations where the transmit and receive antenna arrays are distant from the RIS beyond a wavelength, a reduced model provides accurate results for arbitrary RIS unit cell geometry. Importantly, the simplified model configures as a cascaded channel transfer matrix whose mathematical structure is compliant with widely accepted, but less accurate, system level RIS models. A numerical validation of the communication model is presented for the design of binary RIS structures with scatterers of canonical geometry. Attained results are consistent with path-loss models adopted in communication system design, and have been validated with full-wave simulations. Our results shows that the applicability of communication models based on mutual impedance matrices is not restricted to canonical minimum scattering RIS unit cells.

Index Terms—Method-of-Moment, MIMO, RIS, Meta-surface, Channel capacity, Optimisation

I. INTRODUCTION

RECONFIGURABLE intelligent surfaces (RIS) provide a viable technology for molding the flow of electromagnetic wave energy within arbitrary propagation environments [1]. Wave control capabilities demonstrated by the RIS include anomalous reflection, beam-forming, focusing, and defocusing [2]. Their operation has been studied in free-space, both near-field and far-field [3], [4], as well as in indoor and outdoor environments [5]. The modelling of RIS-assisted wireless links have become a topic of paramount importance [6], and several authors have proposed physics-based communications models [7].

The scientific literature classifies first-principle electromagnetics model of the RIS in two families: Continuous and Discrete models [8]. Continuous models treat meta-surfaces as homogenous sheets of currents whole effective impedance and admittance are matched by design to perform anomalous reflection. Discrete models treat individual pixels: In the first models inspired from antenna arrays, the effective scattered field results from the superposition of waves re-radiated upon

K. Konno and Q. Chen are with the Department of Communications Engineering, Graduate School of Engineering, Tohoku University, Japan (e-mail:konno@ecei.tohoku.ac.jp).

S. Terranova is with the School of Mathematical Sciences, University of Nottingham, United Kingdom (e-mail:sergio.terranova@nottingham.ac.uk).

G. Gradoni is with the 6G Innovation Centre, Institute for Communication Systems, University of Surrey, United Kingdom (e-mail:g.gradoni@surrey.ac.uk). He is also with the Department of Computer Science and Technology, University of Cambridge, United Kingdom.

Manuscript received June 31, 2023; revised ???? ??, 2023.

specular reflection of individual RIS unit cells. However, it has been shown that effective models based on re-radiated fields: i) do not correctly capture the mutual coupling between unit cells within finite size RIS structures [9], [10]; ii) do rely on local periodicity which provides an approximate behaviour of the field re-radiated by finite-size macro cells [11]; iii) do not accurately capture the effect of loading circuitry on the re-radiated field, as well as parasitic effects within the unit cell [12]. More recently, in order to overcome these limitations, discrete models of the RIS have been formulated by using both impedance [13] and scattering [14] matrix formalisms. Those models are capable of treating a finite-size RIS, capturing joint amplitude and phase variability of the RIS unit cell response, and providing an end-to-end (E2E) representation of the wireless link, i.e., include the interaction of the RIS with the transmit and receive arrays associated to the base-station (BS) to user-equipment (UE) respectively. A specific impedance-based channel model has been formulated for arrays of dipoles [15], and exploited to analyse the benefit of the knowledge of mutual coupling between dipoles in channel gain optimisation [19]. While the model works in both near- and far-field, the RIS unit cell has been assumed to be a minimal scattering linear antenna, for which the surface current density is known in closed form and the array active impedance can be computed efficiently including mutual coupling [24]. The structural scattering of the open-circuit [21] baseline RIS structure needs to be considered and included in impedance-based models. We extend the model in [15] to arbitrary arrays of scatterers adopted for RIS using the Method-of-Moment (MoM) formalism. The MoM code that we use has been recently developed in [27], which has used the methodology originally proposed in the theory of loaded scatterers [21], where port segments have been separated from passive segments in the MoM discretisation. A MoM study has been recently proposed for the path loss of a RIS-assisted SISO system, where freestanding loaded loops have been assumed as RIS unit cells [28].

In our MoM model, the ground plane has been included and the formulation is amenable to accounting for single- as well as multi-layer substrates by using standard methodologies [43]. Furthermore, our model provides an end-to-end communication model that can be conveniently used for optimisation and performance analysis of wireless links, and it naturally extends the model in [15] beyond the canonical minimum scattering (CMS) approximation. This extension has the benefit of making important work on CMS structures practical: This work has been achieved in the literature lately,

also considering wide-band response of linear antennas [16], and including e.g., multi-path fading generated by clusters of dipoles in the impedance [17] and the Green function [18] formalisms. Previous studies have discussed the inclusion of circuital elements within periodic meta-surfaces with sub-wavelength unit cells in MoM [25], There, a simple development of the MoM interaction matrix allowed the computation of the scattered field for arbitrary distribution of discrete loads. This boils down to add the impedance matrix of the equivalent circuit of the tunable elements to the MoM interaction impedance matrix of port basis segments. In RIS design, it is worth noticing that the inner coupling between loading circuitry and planar metallic structure might generate parasitic effects, which are usually captured by a more complicated (and structure dependent) equivalent circuit [26]. In the far-field of a single RIS unit cell, our model reduces to a cascaded formula that has the same mathematical structure of system levels MIMO communication models [15]. However, the impedance matrix is augmented with the self- and mutual- interactions involving scattering segments besides port segments. Importantly, while system level models are not constructed in physics-based grounds and are prone to efficient optimisation, our electromagnetic compliant model preserves accuracy for arbitrary RIS unit cell geometry. A numerical analysis of the the simplified communication model has been carried out for two canonical unit cell geometries, and validated by the (related) exact MoM code. The performance of a compact RIS-assisted MIMO link is also assessed in terms of channel capacity.

The paper is organised as follows, in Sec. II we apply the method-of-moment formulation to the communication system including the RIS, transmit and receive arrays. We partition basis functions into port and passive segments. We then devise an end-to-end communication model, and devise a reduced cascaded model. In Sec. III we design two RIS structures based on loaded scatterers, and we assess the model by numerical validations of the channel capacity at variable receiver distance and direction. Finally, in Sec. IV we draw a conclusion and future perspectives.

II. FORMULATION

Here, a channel matrix between ports of transmitting and receiving antennas is formulated using an impedance (admittance) matrix obtained using method of moments (MoM). Formulation using MoM is different from that using z-parameters between ports because impedance matrix entries are defined between segments, where segments are part of antennas or scatterers whose current distribution is expanded by basis functions. However, according to definition of the z-parameters, the z-parameters between ports are available from matrix equations formulated using MoM. In the same manner as the z-parameters between ports, channel matrix between ports is also available from matrix equations formulated using MoM.

A. Full-wave model

Here, an equivalent circuit of RIS including transmitting/receiving antennas is modeled via method of moments
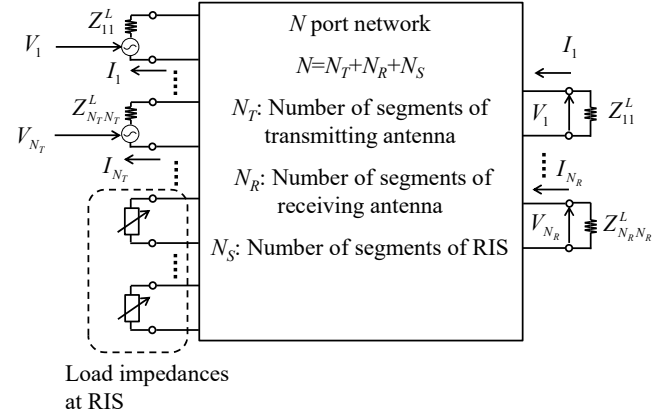

Fig. 1. Equivalent circuit of RIS including transmitting/receiving antennas.

(MoM) as shown in Fig. 1. The equivalent circuit is expressed as a matrix equation as follows.

$$(\mathbf{Z}_{N \times N} + \mathbf{Z}_{N \times N}^L)\mathbf{I}_N = \mathbf{V}_N \qquad (1)$$

Here, $\mathbf{Z}_{N \times N}$ is $N \times N$ impedance matrix, $\mathbf{Z}_{N \times N}^L$ is $N \times N$ load impedance matrix, $\mathbf{I}_N$ is N dimensional current vector, and $\mathbf{V}_N$ is N dimensional voltage vector, and N is the total number of segments (i.e. number of unknowns).

Equation (1) can be partitioned using block matrices/vectors as follows.

$$
\left[\begin{array}{c} \mathbf{V}_{N_T} \\ 0 \\ 0 \end{array} \right] = \left[\begin{array}{cc} \mathbf{Z}_{N_T \times N_T} + \mathbf{Z}_{N_T \times N_T}^L & \mathbf{Z}_{N_T \times N_R} \\ \mathbf{Z}_{N_R \times N_T} & \mathbf{Z}_{N_R \times N_R} + \mathbf{Z}_{N_R \times N_R}^L \\ \mathbf{Z}_{N_S \times N_T} & \mathbf{Z}_{N_S \times N_R} \end{array} \right.
$$
$$
\left. \begin{array}{c} \mathbf{Z}_{N_T \times N_S} \\ \mathbf{Z}_{N_R \times N_S} \\ \mathbf{Z}_{N_S \times N_S} + \mathbf{Z}_{N_S \times N_S}^L \end{array} \right] \left[\begin{array}{c} \mathbf{I}_{N_T} \\ \mathbf{I}_{N_R} \\ \mathbf{I}_{N_S} \end{array} \right] \qquad (2)
$$

Here, N_T is the number of segments of transmitting antennas, N_R is the number of segments of receiving antennas, and N_S is the number of segments of scatterers with variable load impedance (i.e. $N_T + N_R + N_S = N$). $\mathbf{Z}_{i \times j}$ is $i \times j$ block impedance matrix, where $i = N_T, N_R, N_S$ and $j = N_T, N_R, N_S$. $\mathbf{Z}_{N_T \times N_T}^L$ is a $N_T \times N_T$ diagonal matrix corresponding to transmitting antennas and includes their load impedance connected to the ports. $\mathbf{Z}_{N_R \times N_R}^L$ is a $N_R \times N_R$ diagonal matrix corresponding to receiving antennas and includes their load impedance connected to the ports. $\mathbf{Z}_{N_S \times N_S}^L$ is a $N_S \times N_S$ diagonal matrix corresponding to scatterers with variable load impedance and includes their load impedance connected to the ports. $\mathbf{I}_{N_T}$, $\mathbf{I}_{N_R}$, and $\mathbf{I}_{N_S}$ are N_T, N_R and N_S dimensional block current vectors. $\mathbf{V}_{N_T}$ is a N_T dimensional block voltage vector corresponding to the segments of the transmitting antennas. A voltage-voltage MIMO channel matrix, compliant to that used in wireless system optimization [19], [20], is derived from the transfer matrix partitioning introduced in (2), which is based on [21], and described in Appendix A. It configures as

$$\mathbf{V}_{N_R} = \mathbf{Z}_{N_R \times N_R}^L \mathbf{I}_{N_R} \qquad (3)$$
$$= \mathbf{H}_{N_R \times N_T}^f \mathbf{V}_{N_T} \qquad (4)$$

with

$$
\begin{aligned}
\mathbf{H}^f_{N_R \times N_T} = \mathbf{Z}^L_{N_R \times N_R}(\mathbf{U}_{N_R \times N_R} + \mathbf{Z}^L_{N_R \times N_R}(\mathbf{Y}_{N_R \times N_R} \\
- \mathbf{Y}_{N_R \times N_S}\mathbf{Z}^L_{N_S \times N_S}(\mathbf{U}_{N_S \times N_S} + \mathbf{Y}_{N_S \times N_S} \\
\mathbf{Z}^L_{N_S \times N_S})^{-1}\mathbf{Y}_{N_S \times N_R}))^{-1}(\mathbf{Y}_{N_R \times N_T} - \mathbf{Y}_{N_R \times N_S} \\
\mathbf{Z}^L_{N_S \times N_S} \times (\mathbf{U}_{N_S \times N_S} + \mathbf{Y}_{N_S \times N_S}\mathbf{Z}^L_{N_S \times N_S})^{-1} \\
\mathbf{Y}_{N_S \times N_T})
\end{aligned} \tag{5}
$$

It is worth noticing that $\mathbf{V}_{N_R}$ is a receiving voltage vector and entries of $\mathbf{H}^f_{N_R \times N_T}$ - corresponding to the ports of the transmitting/receiving antennas - are extracted to obtain complex-valued channel gains [22]. The channel matrix obtained from (5) is a full-wave expression as no approximation is introduced through its derivation. Finally, we have verified that the channel matrix obtained from (5) perfectly agrees with that obtained by full-wave analysis. Interestingly, the impedance formulation in (5) does not configure as a cascaded model and it presents inverse operators that cannot be expanded in Neumann series since their spectral radius is not smaller than the unity. Hence, we support the observation done in [23] concerning the mathematical structure of the scattering formulation, whose spectral radius is smaller than the unity thus allowing for a Born series type expansion, while the impedance formulation does not allow for such an expansion.

B. Reduced model

Here, it is assumed that effect of mutual coupling among the transmitting antennas, receiving antennas, and the RIS is negligible when their current distribution is obtained (The assumption is reasonable when they are in far-field region.). According to the assumption, current distribution of the transmitting antennas are approximately obtained from Eq. (2) as follows.

$$
\begin{aligned}
\mathbf{V}_{N_T} &= (\mathbf{Z}_{N_T \times N_T} + \mathbf{Z}^L_{N_T \times N_T})\mathbf{I}_{N_T} + \mathbf{Z}_{N_T \times N_R}\mathbf{I}_{N_R} \\
&\quad + \mathbf{Z}_{N_T \times N_S}\mathbf{I}_{N_R} \\
&\approx (\mathbf{Z}_{N_T \times N_T} + \mathbf{Z}^L_{N_T \times N_T})\mathbf{I}_{N_T} \\
\mathbf{I}_{N_T} &\approx (\mathbf{Z}_{N_T \times N_T} + \mathbf{Z}^L_{N_T \times N_T})^{-1}\mathbf{V}_{N_T}
\end{aligned} \tag{6}
$$

Next, current distribution of the RIS is obtained. According to the third column of Eq. (2), current distribution of RIS is approximately obtained as follows.

$$
\begin{aligned}
0 &= \mathbf{Z}_{N_S \times N_T}\mathbf{I}_{N_T} + \mathbf{Z}_{N_S \times N_R}\mathbf{I}_{N_R} + (\mathbf{Z}_{N_S \times N_S} + \mathbf{Z}^L_{N_S \times N_S})\mathbf{I}_{N_S} \\
&\approx \mathbf{Z}_{N_S \times N_T}\mathbf{I}_{N_T} + (\mathbf{Z}_{N_S \times N_S} + \mathbf{Z}^L_{N_S \times N_S})\mathbf{I}_{N_S} \\
\mathbf{I}_{N_S} &= -(\mathbf{Z}_{N_S \times N_S} + \mathbf{Z}^L_{N_S \times N_S})^{-1}\mathbf{Z}_{N_s \times N_T}\mathbf{I}_{N_T} \\
&= -(\mathbf{Z}_{N_S \times N_S} + \mathbf{Z}^L_{N_S \times N_S})^{-1}\mathbf{Z}_{N_s \times N_T} \\
&\quad (\mathbf{Z}_{N_T \times N_T} + \mathbf{Z}^L_{N_T \times N_T})^{-1}\mathbf{V}_{N_T} \quad (\because \text{Eq.}(6))
\end{aligned} \tag{7}
$$

After that, current distribution of the receiving antennas is approximately obtained from the second column of Eq. (2)

with the help of Eqs. (6) and (7).

$$
\begin{aligned}
0 &= \mathbf{Z}_{N_R \times N_T}\mathbf{I}_{N_T} + (\mathbf{Z}_{N_R \times N_R} + \mathbf{Z}^L_{N_R \times N_R})\mathbf{I}_{N_R} \\
&\quad + \mathbf{Z}_{N_R \times N_S}\mathbf{I}_{N_S} \\
\mathbf{I}_{N_R} &= -(\mathbf{Z}_{N_R \times N_R} + \mathbf{Z}^L_{N_R \times N_R})^{-1} \\
&\quad (\mathbf{Z}_{N_R \times N_T}\mathbf{I}_{N_T} + \mathbf{Z}_{N_R \times N_S}\mathbf{I}_{N_S}) \\
&= -(\mathbf{Z}_{N_R \times N_R} + \mathbf{Z}^L_{N_R \times N_R})^{-1}(\mathbf{Z}_{N_R \times N_T}(\mathbf{Z}_{N_T \times N_T} \\
&\quad + \mathbf{Z}^L_{N_T \times N_T})^{-1}\mathbf{V}_{N_T} - \mathbf{Z}_{N_R \times N_S}(\mathbf{Z}_{N_S \times N_S} + \mathbf{Z}^L_{N_S \times N_S})^{-1} \\
&\quad \mathbf{Z}_{N_s \times N_T}(\mathbf{Z}_{N_T \times N_T} + \mathbf{Z}^L_{N_T \times N_T})^{-1}\mathbf{V}_{N_T}) \\
&= (\mathbf{Z}_{N_R \times N_R} + \mathbf{Z}^L_{N_R \times N_R})^{-1}(-\mathbf{Z}_{N_R \times N_T} + \mathbf{Z}_{N_R \times N_S} \\
&\quad (\mathbf{Z}_{N_S \times N_S} + \mathbf{Z}^L_{N_S \times N_S})^{-1}\mathbf{Z}_{N_s \times N_T}) \\
&\quad \times (\mathbf{Z}_{N_T \times N_T} + \mathbf{Z}^L_{N_T \times N_T})^{-1}\mathbf{V}_{N_T}
\end{aligned} \tag{8}
$$

The receiving voltage vector $\mathbf{V}_{N_R}$ of the receiving antennas is expressed as follows.

$$
\mathbf{V}_{N_R} = \mathbf{Z}^L_{N_R \times N_R}\mathbf{I}_{N_R} = \mathbf{H}_{N_R \times N_T}\mathbf{V}_{N_T} \tag{9}
$$

where the voltage-voltage MIMO channel matrix is obtained as

$$
\begin{aligned}
\mathbf{H}_{N_R \times N_T} &= \mathbf{Z}^L_{N_R \times N_R}(\mathbf{Z}_{N_R \times N_R} + \mathbf{Z}^L_{N_R \times N_R})^{-1} \\
&\quad \times (-\mathbf{Z}_{N_R \times N_T} + \mathbf{Z}_{N_R \times N_S}\, \Phi_S\, \mathbf{Z}_{N_s \times N_T}) \\
&\quad \times (\mathbf{Z}_{N_T \times N_T} + \mathbf{Z}^L_{N_T \times N_T})^{-1}\mathbf{V}_{N_T}
\end{aligned} \tag{10}
$$

and the RIS state matrix is given by the admittance matrix

$$
\Phi_S = (\mathbf{Z}_{N_S \times N_S} + \mathbf{Z}^L_{N_S \times N_S})^{-1} \tag{11}
$$

which is consistent with the communication model in [15] in the far-field approximation, that has been used in sum-rate optimization [20]. Because the block load impedance matrix $\mathbf{Z}^L_{N_R \times N_R}$ is a diagonal matrix, its entries are zero except for the ports of the receiving antennas. Finally, entries of $\mathbf{H}_{N_R \times N_T}$ corresponding to the ports of the transmitting/receiving antennas are extracted and the channel matrix is obtained.

C. Structural scattering

In NLOS between transmit and receive array, the cascaded communication model in [15] vanishes if all the dipole ports are in open circuit, on account of the minimum scattering assumption [29]. Importantly, the MoM based formulation leads to a non-zero RIS state matrix when unit cells are unloaded. The reason lies in the presence of passive segments that capture the structural scattering of the bare metasurface structure. This can be seen by considering the active impedance of a single unit cell of the RIS. Suppose we have a linear antenna discretised by three adjacent segments, of which only one embeds port terminals. Adopting the MoM formalism, the RIS state matrix for the three segments is found from

$$
\mathbf{Z}_{N_S \times N_S} = \begin{pmatrix} Z & Z_c & Z_c \\ Z_c & Z_p & Z_c \\ Z_c & Z_c & Z \end{pmatrix} \tag{12}
$$

where, without loss of generality, mutual coupling impedance Z_c has been assumed uniform within the macro-pixel, with
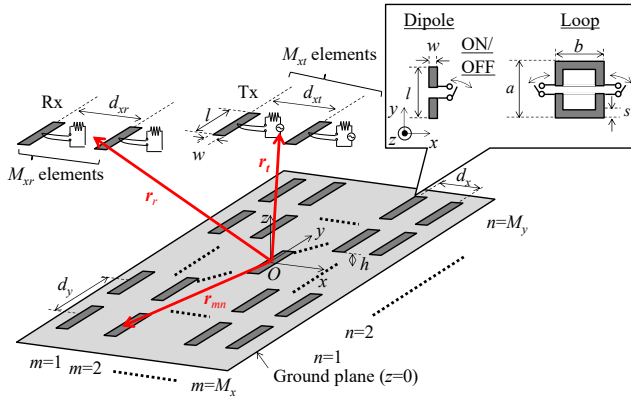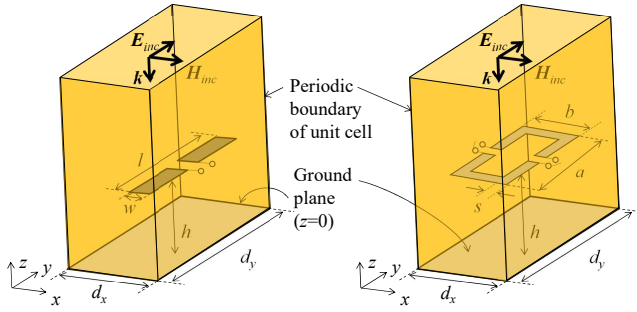
Fig. 2. Geometry of RIS

Fig. 3. Unitcell model of infinite array of RIS elements over PEC ground plane (Left: Planar dipole elements, Right: Rectangular loop elements).

input impedance at the port segment Z_p and at the passive segments Z. The load impedance at the port segment reads

$$\mathbf{Z}^L_{N_S \times N_S} = \begin{pmatrix} 0 & 0 & 0 \\ 0 & Z_L & 0 \\ 0 & 0 & 0 \end{pmatrix} \tag{13}$$

Inserting (12) and (13) in (11) yields the matrix inversion

$$\Phi_S = \begin{pmatrix} Z & Z_c & Z_c \\ Z_c & Z_p + Z_L & Z_c \\ Z_c & Z_c & Z \end{pmatrix}^{-1} \tag{14}$$

which gives, in the open circuit (oc) case, i.e., $Z_L \to \infty$

$$\Phi_S^{oc} = \begin{pmatrix} \frac{Z}{Z^2 - Z_c^2} & 0 & \frac{Z_c}{Z^2 - Z_c^2} \\ 0 & 0 & 0 \\ \frac{-Z_c}{Z^2 - Z_c^2} & 0 & \frac{Z}{Z^2 - Z_c^2} \end{pmatrix} \tag{15}$$

that encodes the passive scattering of the planar structure. Note that differently from [15], the RIS state admittance does not go to zero for unloaded unit cells, which was a consequence of the CMS approximation.

III. NUMERICAL RESULTS

A. Design of RIS

Here, it is demonstrated that our proposed expression works for calculating channel capacity between transmitting and receiving antennas in the presence of RIS. Geometry of the RIS is shown in Fig. 2. Here, either of planar dipole element
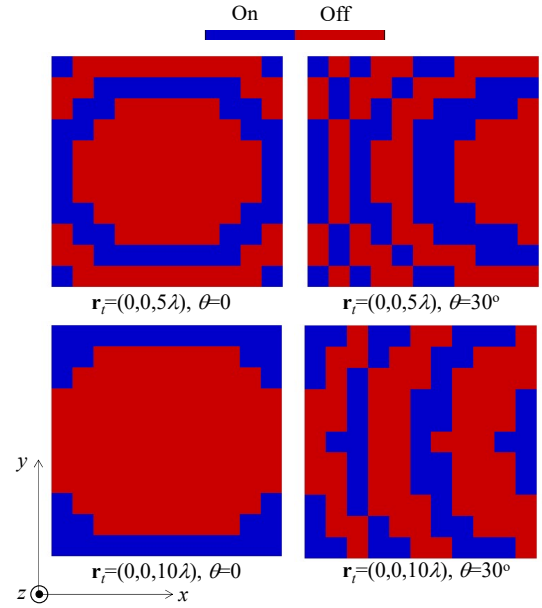

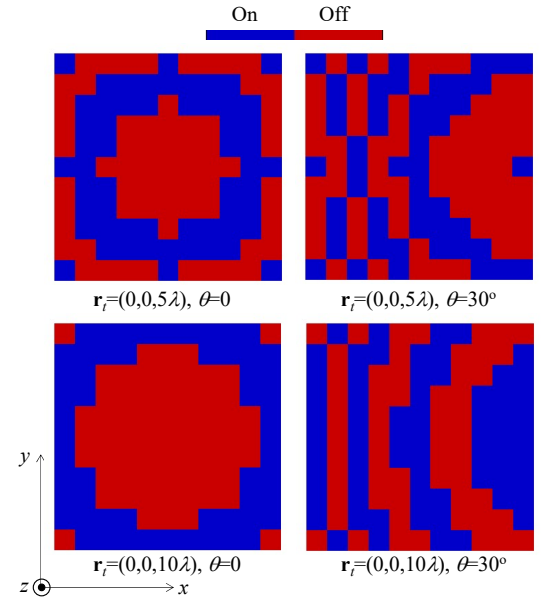Fig. 4. On/off states of RIS elements composed of dipole elements.

Fig. 5. On/off states of RIS elements composed of loop elements.

or planar loop element is used as RIS element. Phase of scattering field of the RIS elements is tunable by variable load impedances. Variable load impedances loaded with RIS elements are simply modeled as open or short terminations, i.e. the RIS is a so-called single bit RIS. Transmitting and receiving antennas are planar dipole array antennas. Origin of the coordinate system is corresponding to the center of the RIS and a position vector pointing the center of the mnth RIS element is $\mathbf{r}_{mn}$. A position vector pointing the center of the transmitting antenna is $\mathbf{r}_t$ and that pointing the center of the receiving antenna is $\mathbf{r}_r$. All of the antenna elements and RIS elements are discretized into triangular segments and their current distribution is expanded using Rao-

TABLE I
PHASE OF REFLECTION COEFFICIENT OF PLANAR DIPOLE AND PLANAR LOOP ELEMENTS.

Type of elements and their dimensions		Planar dipole ($l = 0.5\lambda, w = 0.01\lambda$, $h = 0.25\lambda, d_x = 0.5\lambda$, $d_y = 0.7\lambda$)	Planar loop ($a = b = 0.4\lambda, s = 0.01\lambda$, $h = 0.25\lambda, d_x = d_y = 0.6\lambda$)
Phase of reflection coefficient [deg.]	On state (Short termination)	6.4	-56
	Off state (Open termination)	164.6	122.8

TABLE II
DIMENSIONS OF THE RIS AND TRANSMITTING/RECEIVING ANTENNAS.

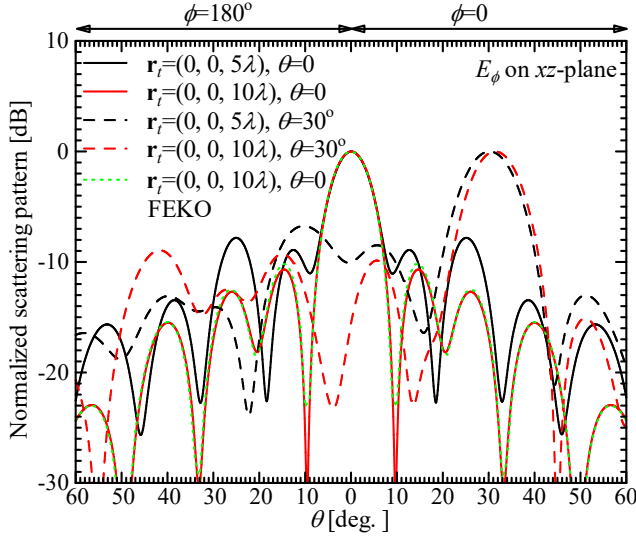| RIS				Tx antenna		Rx antenna	
Planar dipole elements		Planar loop elements					
l	0.5λ	$a = b$	0.4λ	l	0.5λ	l	0.5λ
w	0.01λ	s	0.01λ	w	0.01λ	w	0.01λ
d_x	0.5λ	d_x	0.6λ	d_{xt}	0.5λ	d_{xr}	0.5λ
d_y	0.7λ	d_y	0.6λ	M_{xt}	2	M_{xr}	2
h	0.25λ	h	0.25λ	$\mathbf{r}_t$	$(0, 0, 5\lambda)$	$\mathbf{r}_r$	$(R\cos\theta, 0, R\sin\theta)$
$M_x = M_y$	11	$M_x = M_y$	11		$(0, 0, 10\lambda)$		$\theta = 0, 30°$

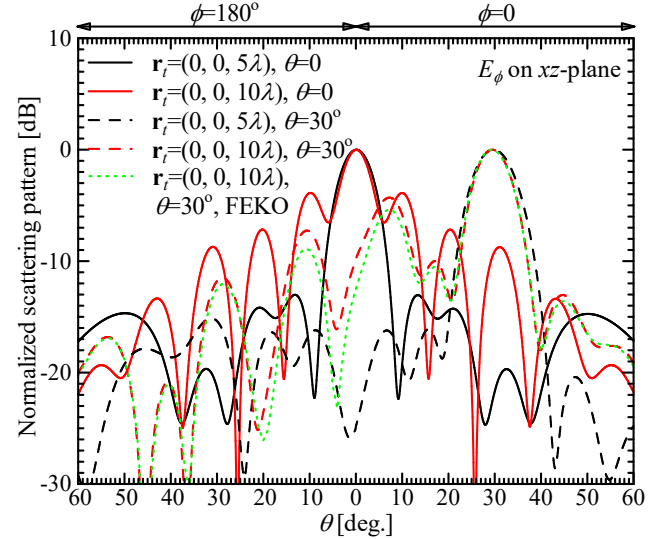Fig. 6. Scattering patterns of RIS composed of dipole elements.

Fig. 7. Scattering patterns of RIS composed of loop elements.

Wilton-Glisson (RWG) basis function [30]. During numerical simulation, geometries of the transmitting/receiving antennas and the RIS are normalized by wavelength λ at their working frequency band.

In advance of designing the RIS, phase of reflection coefficient of the RIS elements is obtained numerically. Here, method of moments based on periodic Green's function (PGF) is used for numerical analysis of the RIS elements in an infinite periodic array [31], [32]. Therefore, the RIS is modeled here as an infinite periodic array whereas the RIS is modeled as a finite periodic array when the channel capacity is obtained later. Poor convergence of the PGF is enhanced by introducing Ewald transformation with the optimum splitting parameter [33]- [35]. Singularity at a point where the source/observation points are is overlapping is annihilated using L'Hospital rule [36], [37].

The geometry of unit cell model composed of planar dipole

elements and planar loop elements is shown in Fig. 3. Phase of reflection coefficient of the unit cell model is obtained for plane wave of normal incidence and is shown in Table I. According to the Table I, it is found that phase shift of 180 deg. is approximately available by switching variable load impedances from on to off, and vice versa. Therefore, it can be said that the planar dipole elements and planar loop elements with variable load impedances are applicable to a single-bit RIS.

The single-bit RIS is designed using the planar dipole elements and planar loop elements. Based on the phase of reflection coefficient, on/off states of the RIS elements are designed so that the scattering fields of the RIS elements are superposed with the minimum error at specific main beam direction. Here, dimensions of the RIS and transmitting antennas are shown in TABLE II. The RIS is designed so that its main beam is directed to $\theta = 0, 30°$. It is worth noticing
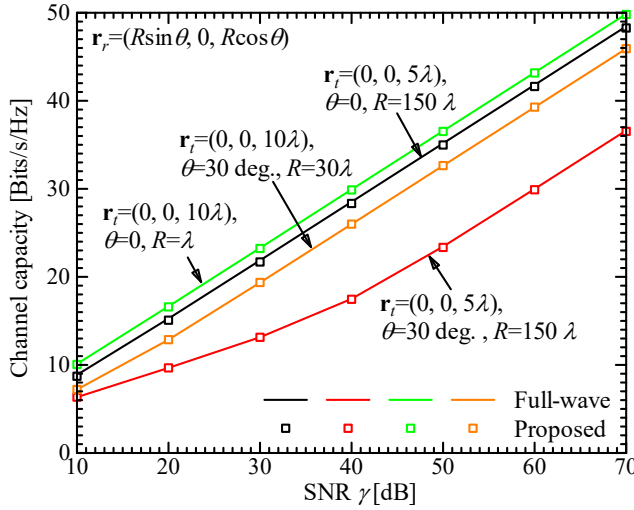
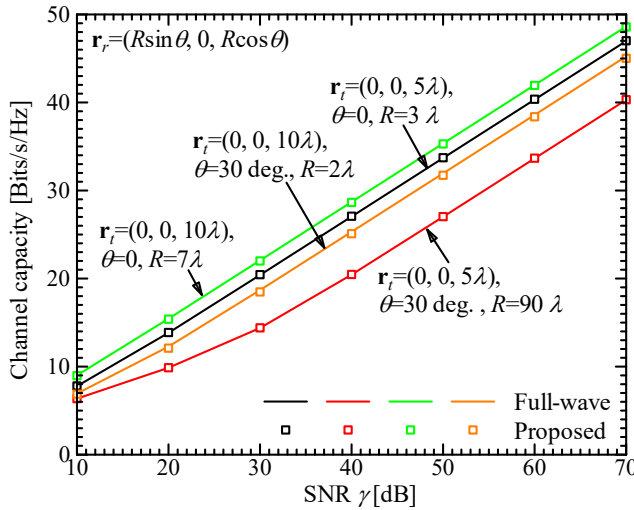Fig. 8.   Channel capacity of RIS composed of planar dipole elements.

Fig. 9.   Channel capacity of RIS composed of planar loop elements.

that this paper focuses on a single beam RIS and a multi beam RIS is beyond the scope of this paper although the proposed method is applicable to numerical analysis of multi beam RIS. Although performance of the proposed method is demonstrated by numerical analysis of the RIS illuminated from broadside angle and focusing on broadside (or off broadside) angle, numerical results in this paper validate performance of the proposed method for numerical analysis of the RIS illuminated from off broadside angle and focusing on (off) broadside angle because of reciprocity.

The RIS is analysed using the MoM with the layered media Green's function(LMGF) and infinite ground plane of the RIS is modeled using the LMGF [38]. Here, the RIS is modeled as a finite periodic array whereas the RIS is modeled as an infinite periodic array when the phase of reflection coefficient was obtained earlier. A direct wave component is extracted from the LMGF and calculated in the spatial domain so that the convergence of the LMGF is enhanced [39], [40]. Sin-

gularity at a point where the source/observation points are is overlapping is annihilated using coordinate transformation and analytic integral [41], [42]. So-called Sommerfeld integral in the LMGF is performed efficiently via numerical interpolation by using Taylor expansions [43], [44].

On/off states of the RIS elements are shown in Figs. 4 and 5. It is found that on/off states of the RIS elements are switched corresponding to the main beam direction or position of the transmitting antenna. The typical phase mask of a lens emerges upon RIS unit cell optimization in both dipole and loop based reflecting surfaces. Normalised scattering patterns of the RISs composed of the planar dipole elements and the planar loop elements are obtained by the MoM, and are shown in Figs. 6 and 7, respectively. It is found that main beam of the RIS is directed to the specific angle because on/off states of the RIS elements are switched so that their scattering fields are with the minimum error at the direction.

B. Channel capacity

Here, it is demonstrated that our proposed expression of the channel capacity is applicable to a wireless communication system including RIS. Dimensions of the transmitting/receiving antennas and the RIS are shown in Table II. The channel capacity is expressed as follows.

$$C = \log_2 \left| \mathbf{I} + \mathbf{H}\mathbf{H}^\dagger \frac{P_t}{M_{xt}\sigma_0^2} \right| \qquad (16)$$

$$= \log_2 \left| \mathbf{I} + \tilde{\mathbf{H}}\tilde{\mathbf{H}}^\dagger \frac{\gamma}{M_{xt}} \right| \qquad (17)$$

where, $\mathbf{I}$ is the unity matrix, $\mathbf{H}$ is a $M_{tr} \times M_{xr}$ channel matrix extracted from $\mathbf{H}_{N_R \times N_T}$, P_t is the total transmitted power, and σ_0^2 is noise power at the receiving antennas. Furthermore, $\tilde{\mathbf{H}}$ is the normalized channel matrix and $\gamma = \frac{P_t\|\mathbf{H}\|^2}{M_{tr}M_{xr}\sigma_0^2}$ is signal-to-noise ratio (SNR) at the receiving antennas [45], [46]. Here, the normalization is performed so that $||\tilde{\mathbf{H}}|| = M_{xt}M_{xr}$ and γ is the SNR per receiving antenna from all transmitting antennas.

As mentioned previously, the reduced model ignores a part of mutual coupling between transmitting/receiving antennas and RIS. Therefore, the reduced model may not be applicable when mutual coupling between transmitting/receiving antennas and RIS is strong, e.g. transmitting/receiving antennas and RIS are close. In order to validate the reduced model from the viewpoint, channel capacity is obtained from small R to large R, where R is spacing from center of the RIS to the receiving antennas. Simulated channel capacity is shown in Figs. 8 and 9 for the RIS composed of the planar dipole/loop array antennas, respectively. Here, the channel capacity was obtained by full-wave analysis (i.e. (2) is solved numerically and the channel matrix is obtained from $\mathbf{V}_{N_T}$ and $\mathbf{I}_{N_R}$).) and by (10), respectively. The scaling laws of the channel capacity with distance are retrieved from the asymptotic expressions of mutual impedances in the far field, which is discussed in [47]. Furthermore, far field behavior of MoM matrices scales with the inverse of the distance as shown in [48, Eq. (17)]. This behavior is consistent (and provides a link) with path-loss

TABLE III
RECIPROCITY AND SYMMETRY OF CHANNEL MATRIX $\mathbf{H}$ BETWEEN THE TRANSMITTING/RECEIVING ANTENNAS WITH RIS COMPOSED OF DIPOLE ELEMENTS. (DIMENSIONS OF RIS AND TRANSMITTING/RECEIVING ANTENNAS ARE TABULATED IN TABLE II. RIS IS DESIGNED FOR TRANSMITTING/RECEIVING ANTENNAS AT $\mathbf{r}_t = (0, 0, 5\lambda)$ AND $\mathbf{r}_r = (0, 0, 10\lambda)$, RESPECTIVELY.)

| | Entries of channel matrix | | | |
| | (Those corresponding to its reciprocal model) | | | |
	H_{11}	H_{12}	H_{21}	H_{22}
Full-wave	$-0.0062 - j0.014$	$0.0045 - j0.028$	$0.0045 - j0.028$	$-0.0062 - j0.014$
	$(-0.0062 - j0.014)$	$(0.0046 - j0.028)$	$(0.0045 - j0.028)$	$(-0.0062 - j0.014)$
(5)	$-0.0062 - j0.014$	$0.0045 - j0.028$	$0.0045 - j0.028$	$-0.0062 - j0.014$
	$(-0.0062 - j0.014)$	$(0.0046 - j0.028)$	$(0.0045 - j0.028)$	$(-0.0062 - j0.014)$
(10)	$-0.0065 - j0.014$	$0.0040 - j0.028$	$0.0040 - j0.028$	$-0.0065 - j0.014$
	$(-0.0065 - j0.014)$	$(0.0040 - j0.028)$	$(0.0040 - j0.028)$	$(-0.0065 - j0.014)$

models (see for example [49], [50]), and shows the generality of the impedance model for arbitrary RIS structures.

On the other hand, numerical results should be further discussed from the physical point of view. The receiving antennas receive direct wave from the transmitting antenna and scattering wave from the RIS simultaneously. The channel capacity depends on receiving signal level, and phase difference between the direct wave and the scattering wave, that depends on position of the receiving antenna, i.e. R and θ, strongly affects the receiving signal level. Therefore, it is expected that the channel capacity changes as the position of the receiving antenna (i.e. R and θ) changes. The channel capacities shown in Figs. 8 and 9 support the discussion. According to the numerical results and discussions, it can be said that the proposed expression is applicable to calculating the channel capacity between the transmitting/receiving antennas in the presence of the RIS.

Finally, reciprocity and symmetry of (5) and (10) are validated numerically. TABLE III shows numerical examples of a channel matrix between the transmitting/receiving antennas with a RIS composed of the dipole elements. TABLE III includes numerical results obtained by full-wave analysis (i.e. (2) is solved numerically and the channel matrix is obtained from $\mathbf{V}_{N_T}$ and $\mathbf{I}_{N_R}$), (5) and (10). According to TABLE III, it is found that entries of the channel matrix hold reciprocity and symmetry except for small numerical error. It is worth noticing that the reciprocity of the reduced model (10) does not hold rigorously because a part of mutual coupling is neglected in its formulation.

IV. CONCLUSION

We have obtained a cascaded communication model for RIS-assisted wireless links from a first-principle electromagnetic model. The formulation has been achieved by partitioning the interaction matrices of the method-of-moments. We have found that the model configures as a cascaded product of interaction matrices in the far-field of the RIS unit cell. This extends communication models based on impedance matrices that have been originally derived under the canonical minimum scattering approximation. The system-level performance of RIS-assisted end-to-end MIMO communications can be accurately simulated with Method of Moments based channel matrices. Finite-size RIS unit cells with arbitrary geometry and dimensions can be characterised and subsequently optimised to achieve prescribed electromagnetic shaping functions. Future

work is required to devise computationally efficient methods for multilayer and transmissive RIS structures.

APPENDIX A
FULL-WAVE EXPRESSION OF CHANNEL MATRIX

Here, full-wave expression of a channel matrix is derived in the same manner with [27]. Starting from Eq. (2), following expression is obtained.

$$
\begin{bmatrix} \mathbf{V}_{N_T} \\ -\mathbf{Z}^L_{N_R \times N_R} \mathbf{I}_{N_R} \\ -\mathbf{Z}^L_{N_S \times N_S} \mathbf{I}_{N_S} \end{bmatrix} = \begin{bmatrix} \mathbf{Z}_{N_T \times N_T} + \mathbf{Z}^L_{N_T \times N_T} \\ \mathbf{Z}_{N_R \times N_T} & \mathbf{Z}_{N_R \times N_R} \\ \mathbf{Z}_{N_S \times N_T} & \mathbf{Z}_{N_S \times N_R} \end{bmatrix}
$$
$$
\begin{matrix} \mathbf{Z}_{N_T \times N_S} \\ \mathbf{Z}_{N_R \times N_S} \\ \mathbf{Z}_{N_S \times N_S} \end{matrix} \begin{bmatrix} \mathbf{I}_{N_T} \\ \mathbf{I}_{N_R} \\ \mathbf{I}_{N_S} \end{bmatrix} \tag{18}
$$

$$
\mathbf{V}'_N = \mathbf{Z}'_{N \times N} \mathbf{I}_N \tag{19}
$$

Here, $\mathbf{V}'_N \equiv [\mathbf{V}_{N_T}, -\mathbf{Z}^L_{N_R \times N_R} \mathbf{I}_{N_R}, -\mathbf{Z}^L_{N_S \times N_S} \mathbf{I}_{N_S}]^T$ and $\mathbf{Z}'_{N \times N}$ is an $N \times N$ impedance matrix where the block load impedance matrix at the transmitting antenna is embedded. Eq. (19) can be solved by multiplying $\mathbf{Y}_{N \times N} \equiv \{\mathbf{Z}'_{N \times N}\}^{-1}$ with its both sides and following expression is obtained.

$$
\mathbf{I}_N = \mathbf{Y}_{N \times N} \mathbf{V}'_N
$$
$$
\begin{bmatrix} \mathbf{I}_{N_T} \\ \mathbf{I}_{N_R} \\ \mathbf{I}_{N_S} \end{bmatrix} = \begin{bmatrix} \mathbf{Y}_{N_T \times N_T} & \mathbf{Y}_{N_T \times N_R} \\ \mathbf{Y}_{N_R \times N_T} & \mathbf{Y}_{N_R \times N_R} \\ \mathbf{Y}_{N_S \times N_T} & \mathbf{Y}_{N_S \times N_R} \end{bmatrix}
$$
$$
\begin{matrix} \mathbf{Y}_{N_T \times N_S} \\ \mathbf{Y}_{N_R \times N_S} \\ \mathbf{Y}_{N_S \times N_S} \end{matrix} \begin{bmatrix} \mathbf{V}_{N_T} \\ -\mathbf{Z}^L_{N_R \times N_R} \mathbf{I}_{N_R} \\ -\mathbf{Z}^L_{N_S \times N_S} \mathbf{I}_{N_S} \end{bmatrix} \tag{20}
$$

According to Eq. (20), following three block matrix equations are obtained.

$$
\begin{cases} \mathbf{I}_{N_T} = \mathbf{Y}_{N_T \times N_T} \mathbf{V}_{N_T} - \mathbf{Y}_{N_T \times N_R} \mathbf{Z}^L_{N_R \times N_R} \mathbf{I}_{N_R} \\ \qquad - \mathbf{Y}_{N_T \times N_S} \mathbf{Z}^L_{N_S \times N_S} \mathbf{I}_{N_S} \quad (21) \\ \mathbf{I}_{N_R} = \mathbf{Y}_{N_R \times N_T} \mathbf{V}_{N_T} - \mathbf{Y}_{N_R \times N_R} \mathbf{Z}^L_{N_R \times N_R} \mathbf{I}_{N_R} \\ \qquad - \mathbf{Y}_{N_R \times N_S} \mathbf{Z}^L_{N_S \times N_S} \mathbf{I}_{N_S} \quad (22) \\ \mathbf{I}_{N_S} = \mathbf{Y}_{N_S \times N_T} \mathbf{V}_{N_T} - \mathbf{Y}_{N_S \times N_R} \mathbf{Z}^L_{N_R \times N_R} \mathbf{I}_{N_R} \\ \qquad - \mathbf{Y}_{N_S \times N_S} \mathbf{Z}^L_{N_S \times N_S} \mathbf{I}_{N_S} \quad (23) \end{cases}
$$

(23) can be transformed as follows.

$$
\mathbf{I}_{N_S} = (\mathbf{U}_{N_S \times N_S} + \mathbf{Y}_{N_S \times N_S} \mathbf{Z}^L_{N_S \times N_S})^{-1}
$$
$$
(\mathbf{Y}_{N_S \times N_T} \mathbf{V}_{N_T} - \mathbf{Y}_{N_S \times N_R} \mathbf{Z}^L_{N_R \times N_R} \mathbf{I}_{N_R}) \tag{24}
$$

This article has been accepted for publication in IEEE Transactions on Antennas and Propagation. This is the author's version which has not been fully edited and content may change prior to final publication. Citation information: DOI 10.1109/TAP.2024.3417629

IEEE TRANSACTIONS ON ANTENNAS AND PROPAGATION, VOL. ??, NO. ?, ???? 2024

Here, $\mathbf{U}_{N_S \times N_S}$ is $N_S \times N_S$ unit matrix. The next, Eq. (22) can be transformed as follows.

$$\mathbf{I}_{N_R} = (\mathbf{U}_{N_R \times N_R} + \mathbf{Y}_{N_R \times N_R}\mathbf{Z}_{N_R \times N_R}^L)^{-1}$$
$$(\mathbf{Y}_{N_R \times N_T}\mathbf{V}_{N_T} - \mathbf{Y}_{N_R \times N_S}\mathbf{Z}_{N_S \times N_S}^L \mathbf{I}_{N_S}) \qquad (25)$$

Equation (24) is substituted into Eq. (25) and following expression is obtained.

$$\mathbf{I}_{N_R} = (\mathbf{U}_{N_R \times N_R} + \mathbf{Y}_{N_R \times N_R}\mathbf{Z}_{N_R \times N_R}^L)^{-1}(\mathbf{Y}_{N_R \times N_T}\mathbf{V}_{N_T}$$
$$- \mathbf{Y}_{N_R \times N_S}\mathbf{Z}_{N_S \times N_S}^L(\mathbf{U}_{N_S \times N_S} + \mathbf{Y}_{N_S \times N_S}\mathbf{Z}_{N_S \times N_S}^L)^{-1}$$
$$(\mathbf{Y}_{N_S \times N_T}\mathbf{V}_{N_T} - \mathbf{Y}_{N_S \times N_R}\mathbf{Z}_{N_R \times N_R}^L\mathbf{I}_{N_R})) \qquad (26)$$
$$= (\mathbf{U}_{N_R \times N_R} + \mathbf{Y}_{N_R \times N_R}\mathbf{Z}_{N_R \times N_R}^L)^{-1}\{ (\mathbf{Y}_{N_R \times N_T}$$
$$- \mathbf{Y}_{N_R \times N_S}\mathbf{Z}_{N_S \times N_S}^L(\mathbf{U}_{N_S \times N_S} + \mathbf{Y}_{N_S \times N_S}\mathbf{Z}_{N_S \times N_S}^L)^{-1}$$
$$\mathbf{Y}_{N_S \times N_T})\mathbf{V}_{N_T} + \mathbf{Y}_{N_R \times N_S}\mathbf{Z}_{N_S \times N_S}^L(\mathbf{U}_{N_S \times N_S}$$
$$+ \mathbf{Y}_{N_S \times N_S}\mathbf{Z}_{N_S \times N_S}^L)^{-1}\mathbf{Y}_{N_S \times N_R}\mathbf{Z}_{N_R \times N_R}^L\mathbf{I}_{N_R} \}(27)$$

Equation (27) can be solved for $\mathbf{I}_{N_R}$ and $\mathbf{I}_{N_R}$ is obtained as follows.

$$\mathbf{I}_{N_R} = (\mathbf{U}_{N_R \times N_R} + \mathbf{Z}_{N_R \times N_R}^L(\mathbf{Y}_{N_R \times N_R} - \mathbf{Y}_{N_R \times N_S}\mathbf{Z}_{N_S \times N_S}^L$$
$$(\mathbf{U}_{N_S \times N_S} + \mathbf{Y}_{N_S \times N_S}\mathbf{Z}_{N_S \times N_S}^L)^{-1}\mathbf{Y}_{N_S \times N_R}))^{-1}(\mathbf{Y}_{N_R \times N_T}$$
$$- \mathbf{Y}_{N_R \times N_S}\mathbf{Z}_{N_S \times N_S}^L(\mathbf{U}_{N_S \times N_S} + \mathbf{Y}_{N_S \times N_S}\mathbf{Z}_{N_S \times N_S}^L)^{-1}$$
$$\times \mathbf{Y}_{N_S \times N_T})\mathbf{V}_{N_T} \qquad (28)$$

Finally, $\mathbf{Z}_{N_R \times N_R}^L$ is multiplied by both sides of Eq. (28), following expressions are obtained.

$$\mathbf{V}_{N_R} = \mathbf{H}_{N_R \times N_T}^f \mathbf{V}_{N_T} \qquad (29)$$

Here, $\mathbf{V}_{N_R}$ and $\mathbf{H}_{N_R \times N_T}^f$ are defined as in (4) and (5), respectively.

ACKNOWLEDGEMENT

REFERENCES

[1] E. C. Strinati et al., "Wireless Environment as a Service Enabled by Reconfigurable Intelligent Surfaces: The RISE-6G Perspective," 2021 Joint European Conference on Networks and Communications & 6G Summit (EuCNC/6G Summit), Porto, Portugal, 2021, pp. 562-567, doi: 10.1109/EuCNC/6GSummit51104.2021.9482474.

[2] M. Di Renzo et al., "Smart Radio Environments Empowered by Reconfigurable Intelligent Surfaces: How It Works, State of Research, and The Road Ahead," in IEEE Journal on Selected Areas in Communications, vol. 38, no. 11, pp. 2450-2525, Nov. 2020, doi: 10.1109/JSAC.2020.3007211.

[3] H. Zhang, N. Shlezinger, F. Guidi, D. Dardari, Y.C. and Eldar, "6G wireless communications: From far-field beam steering to near-field beam focusing," arXiv preprint arXiv:2203.13035, 2022.

[4] G. Bartoli, A. Abrardo, N. Decarli, D. Dardari, and M. Di Renzo, "Spatial Multiplexing in Near Field MIMO Channels with Reconfigurable Intelligent Surfaces." arXiv preprint arXiv:2212.11057, 2023.

[5] X. Pei et al., "RIS-Aided Wireless Communications: Prototyping, Adaptive Beamforming, and Indoor/Outdoor Field Trials," in IEEE Transactions on Communications, vol. 69, no. 12, pp. 8627-8640, Dec. 2021, doi: 10.1109/TCOMM.2021.3116151.

[6] G. Gradoni, M. Di Renzo, A. Diaz-Rubio, S. Tretyakov, C. Caloz, Z. Peng, A. Alu, G. Lerosey, M. Fink, V. Galdi, and T.J., Cui, "Smart radio environments." arXiv preprint arXiv:2111.08676, 2021.

[7] M. Di Renzo, A. Ahmed, A. Zappone, V. Galdi, G. Gradoni, M. Moccia, and G. Castaldi, G., "Digital reconfigurable intelligent surfaces: On the impact of realistic reradiation models," arXiv preprint arXiv:2205.09799, 2022.

[8] M. Di Renzo, F. H. Danufane, S. Tretyakov, "Communication Models for Reconfigurable Intelligent Surfaces: From Surface Electromagnetics to Wireless Networks Optimization," Proceedings of the IEEE, Vol. 110, No. 9, September 2022.

[9] F. H. Danufane, M. D. Renzo, J. de Rosny and S. Tretyakov, "On the Path-Loss of Reconfigurable Intelligent Surfaces: An Approach Based on Green's Theorem Applied to Vector Fields," in IEEE Transactions on Communications, vol. 69, no. 8, pp. 5573-5592, Aug. 2021.

[10] R. J. Williams, P. Ramírez-Espinosa, J. Yuan and E. de Carvalho, "Electromagnetic Based Communication Model for Dynamic Metasurface Antennas," in IEEE Transactions on Wireless Communications, vol. 21, no. 10, pp. 8616-8630, Oct. 2022.

[11] V. Degli-Esposti, E. M. Vitucci, M. D. Renzo and S. A. Tretyakov, "Reradiation and Scattering From a Reconfigurable Intelligent Surface: A General Macroscopic Model," in IEEE Transactions on Antennas and Propagation, vol. 70, no. 10, pp. 8691-8706, Oct. 2022.

[12] S. V. Hum, M. Okoniewski and R. J. Davies, "Modeling and Design of Electronically Tunable Reflectarrays," in IEEE Transactions on Antennas and Propagation, vol. 55, no. 8, pp. 2200-2210, Aug. 2007.

[13] R. J. Williams, P. Ramírez-Espinosa, J. Yuan and E. de Carvalho, "Electromagnetic Based Communication Model for Dynamic Metasurface Antennas," IEEE Transactions on Wireless Communications, vol. 21, no. 10, pp. 8616-8630, Oct. 2022.

[14] S. Shen, B. Clerckx and R. Murch, R., "Modeling and architecture design of reconfigurable intelligent surfaces using scattering parameter network analysis." IEEE Transactions on Wireless Communications, vol. 21, no. 2, pp.1229-1243, 2022.

[15] G. Gradoni and M. Di Renzo, "End-to-End Mutual Coupling Aware Communication Model for Reconfigurable Intelligent Surfaces: An Electromagnetic-Compliant Approach Based on Mutual Impedances," IEEE Wireless Communications Letters, vol. 10, no. 5, pp. 938-942, May 2021, doi: 10.1109/LWC.2021.3050826.

[16] M. Akrout, F. Bellili, A. Mezghani, and J.A. Nossek, 2023. "Physically Consistent Models for Intelligent Reflective Surface-assisted Communications under Mutual Coupling and Element Size Constraint," arXiv preprint arXiv:2302.11130.

[17] P. Mursia, S. Phang, V. Sciancalepore, G. Gradoni, and M. Di Renzo, 2023. "Modeling and optimization of reconfigurable intelligent surfaces in propagation environments with scattering objects," arXiv preprint arXiv:2302.01739.

[18] R. Faqiri, C. Saigre-Tardif, G. C. Alexandropoulos, N. Shlezinger, M. F. Imani and P. del Hougne, "PhysFad: Physics-Based End-to-End Channel Modeling of RIS-Parametrized Environments With Adjustable Fading," IEEE Transactions on Wireless Communications, vol. 22, no. 1, pp. 580-595, Jan. 2023.

[19] X. Qian and M. D. Renzo, "Mutual Coupling and Unit Cell Aware Optimization for Reconfigurable Intelligent Surfaces," IEEE Wireless Communications Letters, vol. 10, no. 6, pp. 1183-1187, June 2021, doi: 10.1109/LWC.2021.3061449.

[20] A. Abrardo, D. Dardari, M. Di Renzo and X. Qian, "MIMO Interference Channels Assisted by Reconfigurable Intelligent Surfaces: Mutual Coupling Aware Sum-Rate Optimization Based on a Mutual Impedance Channel Model," IEEE Wireless Communications Letters, vol. 10, no. 12, pp. 2624-2628, Dec. 2021, doi: 10.1109/LWC.2021.3109017.

[21] J. Mautz and R. Harrington, "Modal analysis of loaded N-port scatterers," in IEEE Transactions on Antennas and Propagation, vol. 21, no. 2, pp. 188-199, March 1973, doi: 10.1109/TAP.1973.1140431.

[22] M. Najafi, V. Jamali, R. Schober and H. V. Poor, "Physics-Based Modeling and Scalable Optimization of Large Intelligent Reflecting Surfaces," IEEE Transactions on Communications, vol. 69, no. 4, pp. 2673-2691, April 2021, doi: 10.1109/TCOMM.2020.3047098.

[23] A. Rabault, L.L. Magoarou, J. Sol, G.C. Alexandropoulos, N. Shlezinger, H.V. Poor, and P. del Hougne, 2023. "On the tacit linearity assumption in common cascaded models of RIS-parametrized wireless channels." arXiv preprint arXiv:2302.04993.

[24] M. Di Renzo, V. Galdi, and G. Castaldi, "Modeling the Mutual Coupling of Reconfigurable Metaurfaces," arXiv preprint arXiv:2210.08619, 2022.

[25] S. Hubert, A. Vallecchi, A. Schuchinsky and C. Craeye, "Modeling of impedance-loaded sub-wavelength metasurfaces," 2017 International Conference on Electromagnetics in Advanced Applications (ICEAA), Verona, Italy, 2017, pp. 1041-1044, doi: 10.1109/ICEAA.2017.8065438.

[26] S. V. Hum, M. Okoniewski and R. J. Davies, "Modeling and Design of Electronically Tunable Reflectarrays," IEEE Transactions on Antennas and Propagation, vol. 55, no. 8, pp. 2200-2210, Aug. 2007, doi: 10.1109/TAP.2007.902002.

[27] K. Konno, Q. Yuan, Q. Chen, K. Yokokawa, J. Goto, and T. Fukawasa, "Efficient Method of Moments for Numerical Analysis of Antennas with Variable Load Impedance," IEEE Trans. Antennas Propag., vol. 68, no. 12, pp. 8233-8237, Dec. 2020.

[28] D. Sarkar, and Y. Antar, "Electromagnetic Insights into Path Loss Modelling of IRS-Assisted SISO Links: Method-of-Moment Based Analysis," Frontiers in Communications and Networks, p.59, 2021.

[29] W. K. Kahn and H. Kurss, "Minimum-scattering antennas," IEEE Transactions on Antennas and Propagation, vol. 13, no. 5, pp. 671-675, September 1965, doi: 10.1109/TAP.1965.1138529.

[30] S. M. Rao, D. R. Wilton, and A. W. Glisson, "Electromagnetic scattering by surfaces of arbitrary shape," IEEE Trans. Antennas Propag., vol. AP-30, no. 3, pp. 409-418, May 1982.

[31] M. G. Floquet, "Sur les équations différentielles linéaires à coefficients périodiques," Annale École Normale Siiperieur, pp. 47-88, 1883.

[32] B. A. Munk, Frequency Selective Surfaces: Theory and Design, New York, NY, USA: Wiley, 2000.

[33] P. P. Ewald, "Dispersion und Doppelbrechung von Elektronengittern (Kristallen)," Dissertation, München, 1912, also Ann. Phys. 49, p. 1, 1916.

[34] P. P. Ewald, "Die Berechnung optischer und elektrostatischer Gitterpotentiale," Ann. Phys. 64, pp. 253–287, 1921.

[35] K. E. Jordan, G. R. Richter, and P. Sheng, "An efficient numerical evaluation of the Green's function for the Helmholtz operator on periodic structures," J. Comp. Phys., vol. 63, pp. 222–235, 1986.

[36] I. Stevanoviæ and J. R. Mosig, "Periodic Green's function for skewed 3-D lattices using the Ewald transformation," Microw. Opt. Tech. Lett., vol. 49, no. 6, pp. 1353-1357, Jun. 2007.

[37] J. Su, X.-W. Xu, M. He, and K. Zhang, "Integral-equation analysis of frequency selective surfaces using Ewald transformation and lattice symmetry" Progress In Electromagnetics Research, vol. 121, pp. 249-269, 2011.

[38] W. C. Chew, Waves and Fields in Inhomogeneous Media, IEEE Press, NY 1995.

[39] W. C. Chew, J. L. Xiong, and M. A. Saville, "A matrix-friendly formulation of layered medium Green's function," IEEE Antennas Wireless Propag. Lett., vol. 5, pp. 490-494, 2006.

[40] Y. P. Chen, W. C. Chew, and L. Jiang, "A new Green's function formulation for modeling homogeneous objects in layered medium," IEEE Trans. Antennas Propag., vol. 60, no. 10, pp. 4766-4776, Oct. 2012.

[41] R. D. Graglia, "On the numerical integration of the linear shape functions times the 3-D Green's function or its gradient on a plane triangle," IEEE Trans. Antennas Propag., vol. 41, no. 10, pp. 1448-1455, Oct. 1993.

[42] D. R. Wilton, S. M. Rao, A. W. Glisson, D. H. Schaubert, O. M. Al-Bundak, and C. M. Butler, "Potential integrals for uniform and linear source distributions on polygonal and polyhedral domains," IEEE Trans. Antennas Propag., vol. 32, no. 3, pp. 276-281, March 1984.

[43] K. Konno, Q. Chen and R.J. Burkholder, "Fast Computation of Layered Media Green's Function via Recursive Taylor Expansion," IEEE Antennas and Wireless Propag. Lett., vol. 16, pp.1048-1051, 2017.

[44] C. A. Balanis, Advanced Engineering Electromagnetics, 2nd ed., John Willey & Sons, pp. 967-979.

[45] S. Loyka and G. Levin, "On physically-based normalization of MIMO channel matrices," IEEE Trans. Wireless Commun., vol. 8, no. 3, pp. 1107-1112, March 2009.

[46] S. S. A. Yuan, X. Chen, C. Huang and W. E. I. Sha, "Effects of Mutual Coupling on Degree of Freedom and Antenna Efficiency in Holographic MIMO Communications," IEEE Open J. Antennas Propag., vol. 4, pp. 237-244, 2023.

[47] M. Akrout, V. Shyianov, F. Bellili, A. Mezghani, and R.W. Heath, 2022. "Super-Wideband Massive MIMO," arXiv preprint arXiv:2208.01556.

[48] C. H. Schmidt, M. M. Leibfritz and T. F. Eibert, "Fully probe-corrected near-field far-field transformation employing plane wave expansion and diagonal translation operators," IEEE Transactions on Antennas and Propagation, vol. 56, no. 3, pp. 737-746, March 2008.

[49] M. Di Renzo, F. Habibi Danufane, X. Xi, J. de Rosny and S. Tretyakov, "Analytical Modeling of the Path-Loss for Reconfigurable Intelligent Surfaces – Anomalous Mirror or Scatterer ?," 2020 IEEE 21st International Workshop on Signal Processing Advances in Wireless Communications (SPAWC), Atlanta, GA, USA, pp. 1-5, 2020.

[50] J. C. B. Garcia, A. Sibille and M. Kamoun, "Reconfigurable Intelligent Surfaces: Bridging the Gap Between Scattering and Reflection," in IEEE Journal on Selected Areas in Communications, vol. 38, no. 11, pp. 2538-2547, Nov. 2020.

Keisuke Konno (M'12) received the B.E., M.E., and D.E. degrees from Tohoku University, Sendai, Japan, in 2007, 2009, and 2012, respectively. Since 2012, he has been with the Department of Communications Engineering, Graduate School of Engineering, Tohoku University, where he is an Associate Professor. He received a JSPS Postdoctral Fellowships for Research Abroad and he was staying with the ElectroScience Laboratory, the Ohio State University, as a visiting scholar from 2015 to 2017. His research interests include computational electromagnetics, array antennas, reflectarrays, and source reconstruction. Dr. Konno is a member of IEEE and IEICE.

He received the Encouragement Award for Young Researcher and Most Frequent Presentations Award in 2010 from the Technical Committee on Antennas and Propagation of Japan, Young Researchers Award in 2011 from the Institute of Electronics, Information and Communication Engineers (IEICE) of Japan, IEEE EMC Society Sendai Chapter Student Brush-up Session & EMC Sendai Seminar Student Best Presentation Award in 2011, JSPS Washington Director Award in 2016, MHz Rectenna Award in 2017, Young Researchers Award for ECEI of Tohoku University in 2018, Minoru Ishida Award in 2018, IEEE AP-S Japan Young Engineer Award in 2018, TOKIN Foundation Research Encouragement Award in 2019, IEICE Communications Society Distinguished Contributions Awards in 2019 and 2021.

Sergio Terranova (M'12) received the Master degrees in telecommunications engineering and the Ph.D. degree in Information Engineering from the University of Pisa, Italy, in 2017, and 2021, respectively. Since 2021 is a research fellow at the School of Mathematical Sciences, University of Nottingham, UK. His research activity is mainly focused on metamaterials, reconfigurable metasurfaces, reconfigurable antennas, additive manufacturing, sensors, radio frequency identification (RFID) systems, Asymptotic Methods in Electromagnetics and Advanced Ray Tracing Methods.

Qiang Chen received the B.E. degree from Xidian University, Xi'an, China, in 1986, the M.E. and D.E. degrees from Tohoku University, Sendai, Japan, in 1991 and 1994, respectively. He is currently Chair Professor of Electromagnetic Engineering Laboratory with the Department of Communications Engineering, Faculty of Engineering, Tohoku University. His primary research interests include antennas, microwave and millimeter wave, electromagnetic measurement and computational electromagnetics.

He received the Best Paper Award and Zen-ichi Kiyasu Award from the Institute of Electronics, Information and Communication Engineers (IEICE). He served as the Chair of IEICE Technical Committee on Photonics-applied Electromagnetic Measurement from 2012 to 2014, the Chair of IEICE Technical Committee on Wireless Power Transfer from 2016 to 2018, the Chair of IEEE Antennas and Propagation Society Tokyo Chapter from 2017 to 2018, the Chair of IEICE Technical Committee on Antennas and Propagation from 2019 to 2021. IEICE Fellow.

Gabriele Gradoni (M'12) received the Ph.D. degree in electromagnetics from Universita Politecnica delle Marche, Ancona, Italy, in 2010. He was a Visiting Researcher with the Time, Quantum, and Electro-magnetics Team, National Physical Laboratory, Teddington, U.K., in 2008. From 2010 to 2013, he was a Research Associate with the Institute for Research in Electronics and Applied Physics, University of Maryland, College Park, MD, USA. From 2013 to 2016, he was a Research Fellow with the School of Mathematical Sciences, University of Nottingham, U.K., where he was a Full Professor of mathematics and electrical engineering. Since May 2023 he has been Full Professor and Chair of Wireless Communications at the 6G Innovation Centre, Institute for Communication Systems, University of Surrey, Guildford, U.K. Since June 2020, he has been an Adjunct Associate Professor with the Department of Electrical and Computer Engineering, University of Illinois at Urbana–Champaign, USA. Since 2020, he has been a Royal Society Industry Fellow at British Telecom, U.K. Since December 2022, he has been a Visiting Fellow with the Department of Computer Science and Technology, University of Cambridge, U.K. His research interests include probabilistic and asymptotic methods for propagation in complex wave systems, metasurface modeling, quantum/wave chaos, and quantum computational electromagnetics, with applications to electro-magnetic compatibility and modern wireless communication systems. He is a member of the IEEE and the Italian Electromagnetics Society.

He received the URSI Commission B. Young Scientist Award in 2010 and 2016, the Italian Electromagnetics Society Gaetano Latmiral Prize in 2015, and the Honorable Mention IEEE TEMC Richard B. Schulz Transactions Prize Paper Award in 2020. From 2014 to 2021, he was the URSI Commission E. Early Career Representative.